Simple, accurate electrostatics-based formulas for calculating ionization potentials, electron affinities, and capacitances of fullerenes

Alexander B. Atanasov and James C. Ellenbogen[*]

Nanosystems Group, The MITRE Corporation, McLean, Virginia 22102, USA

A set of simple analytic formulas is derived via electrostatics-based methods to accurately calculate the values of electron affinities A_n and ionization potentials I_n for n-carbon icosahedral fullerene molecules as a function of their average radii R_n. These formulas reproduce with accuracy the values of A_n, I_n, and their scalings with $1/R_n$ that were determined previously in detailed, computationally intensive density functional theory calculations. The formula for A_n is derived from an enhanced image-charge model that treats the valence region of the icosahedral system as a quasispherical conductor of radius $(R_n + \delta)$, where $\delta = 1/4W_\infty$ is a small constant distance determined from the work function W_∞ of graphene. Using this model, though, a formula for I_n that includes only electrostatics-like terms does not exhibit accuracy similar to the analogous formula for A_n. To make it accurate, a term must be added to account for the large symmetry-induced quantum energy gap in the valence energy levels (i.e., the HOMO-LUMO gap). An elementary two-state model based upon a quantum rotor succeeds in producing a simple expression that evaluates the energy gap as an explicit function of A_n. Adding this to the electrostatics-like formula for I_n gives a simple quantum equation that yields accurate values for I_n and expresses them as a function of A_n. Further, the simple equations for A_n and I_n yield significant insight into both the physics of electron detachment in the fullerenes and the scaling with R_n of their quantum capacitances $C_n = 1/(I_n - A_n)$.

I. INTRODUCTION

Fullerene nanostructures [1,2] are in many ways archetypal carbon particles. Further, carbon particles are at the heart of a number of important electrical energy storage innovations [3,4], while more such innovations are essential to develop and improve a wide variety of other advanced technology products. Thus, it is important to establish a firmer foundation for our prior analysis [5] of how fullerenes store charge and electrical energy, how much they can store, and how that quantity, or capacitance, varies as carbon particles in practical applications are shrunk to the nanoscale to achieve much greater aggregate surface areas. Additionally, the invariance of the local electronic structure and the quasispherical global structure of fullerenes C_n as they vary in carbon number n and average radius R_n makes them ideal for investigating the nature and scaling of quantum properties, such as electron detachment energies. Fullerenes are especially suited for considering scaling that occurs as the sizes of structures cross boundaries that usually are regarded as separating the domain of classical behavior from that of quantum behavior.

Motivated by this coupling of practical concerns and long-term fundamental concerns [5–9], we develop here a very simple set of equations for accurately calculating the values of the electron affinity A_n and the ionization potential I_n for an icosahedral fullerene as a function of R_n. We employ these equations to analyze the scaling of A_n and I_n with $1/R_n$. For it is these electron detachment energies and their scaling that determine the molecules' quantum capacitances [10,11],

$$C_n = 1/(I_n - A_n), \qquad (1)$$

and their linear scaling with R_n [5].

For large molecules, like the fullerenes, I_n and A_n usually are difficult to determine accurately from theory, at least without very computationally intensive *ab initio* or density functional theory (DFT) calculations, such as we collaborated in performing as part of an earlier study [5] of fullerene capacitances. Obtaining accurate electron affinities is particularly challenging, from experiment or from theory.

In this work, though, we discover that we are able to treat neutral fullerene molecules as though they are hollow spherical conductors and we adapt a spherical image-charge model [12–14] from classical electrostatics to derive an analytic equation that evaluates their electron affinities with much accuracy. This can be seen in Fig. 1 for the case of closed-shell icosahedral fullerenes, having the formula C_{60k}, where k is an integer. In the figure, the open circles and their dashed regression line are determined from the above-mentioned electrostatics-like analytic equation we derive for A_n. These points are nearly identical to the filled-circle points and solid regression line plotted from detailed DFT calculations [5] to determine A_n for icosahedral fullerenes.

On the other hand, we found that the usual prescription [13,14] arising from a spherical image-charge model for calculating an ionization potential from an electron affinity is not at all accurate in determining the ionization potentials for icosahedral fullerenes. That is, the detachment energies are all much too small if we start with a neutral fullerene, then remove to $r = \infty$ its highest energy valence electron from a radius $R_n + \delta$ just outside the quasisphere containing the nuclei, while accounting only for: (a) the image charge contribution to the energy of removal, which is identical to A_n, plus (b) a "charging term" $1/(R_n + \delta)$ that arises from the Coulomb attraction of the departing electron to the single positive charge $\zeta = +1$ on the cation it leaves behind. The resulting set of too-small values for the ionization potentials also is seen in Fig. 1, where the open squares and their nearly linear dotted
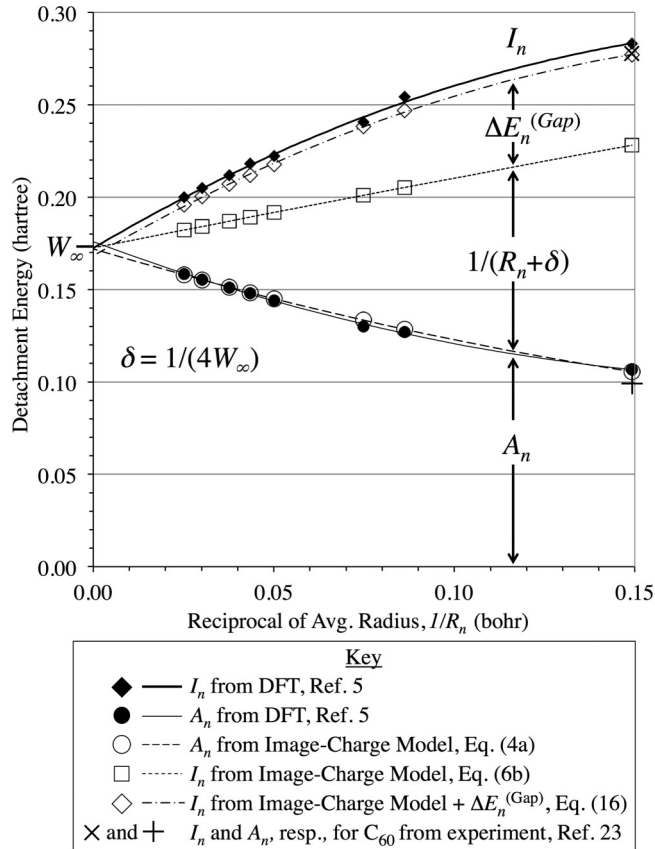
032508-1

FIG. 1. Plot versus $1/R_n$ of icosaheral fullerene electron detachment energies from DFT calculations [5] and from simple formulas derived in this work. Values plotted are given in Table I. Labels of the two-headed arrows correspond to the terms in Eq. (2) that sum to the energies represented by points plotted along the different scaling curves in the graph. Scaling curves are determined via second-order polynomial regression analysis. Notable in the graph are the very close matches of the dashed scaling curves determined from analytical equations derived here with solid curves determined from accurate DFT calculations of detachment energies I_n and A_n.

regression line from this purely image-charge–based approach to I_n are well below the filled diamonds and the solid bold black curved regression line that arise from accurate DFT values.

The discrepancy can be attributed to the fact that the icosahedral fullerenes are not actually spheres and that taking explicit account of their true symmetry splits the energy level in which the highest energy π-electrons would reside. This splitting introduces a large quantum energy gap $\Delta E_n^{(Gap)}$ between the one-electron energy level that corresponds to the highest occupied molecular orbital (HOMO) in the neutral species and its lowest unoccupied molecular orbital (LUMO) [15–20], which also closely approximates the energy level in which the extra electron resides in the anion. This energy gap is present and should be of very nearly the same magnitude in an icosahedral fullerene anion, because the addition of a single electron should have little effect on the valence one-electron energy levels in a molecule with so many valence electrons as a fullerene.

The energy gap is important because the energies of the HOMO and LUMO one-electron states approximate those of

the different energy states from which the first electrons are detached in the neutral and anionic systems, respectively. Thus, to calculate I_n from A_n for an icosahedral fullerene, one must account for this difference and add a corresponding quantum mechanical energy gap term to the two above-described electrostatics-like terms (a) and (b) that arise from a spherical electrostatic model:

$$I_n = A_n + \frac{1}{R_n + \delta} + \Delta E_n^{(Gap)}. \qquad (2)$$

This relation is depicted schematically in Fig. 1.

Above, the parameter δ is a small distance, 1.45 bohr, that can be thought of, classically, as the difference between the average radius R_n for a fullerene and the radius for the attachment or detachment of a valence electron to or from a fullerene [21]. In Eq. (2), the charging energy term that involves δ arises from classical electrostatics and is classical in form. However, δ itself is quantum mechanical in origin in that it represents an average distance outside the surface containing the carbon nuclei at which an electron standing wave is established. The value of δ, which is constant for all n, is determined below from that of W_∞, the work function of graphene.

Even though the energy gap arises from nonspherical symmetry breaking, a second discovery here is that we still can take further advantage of the fact that the fullerene anions and neutral molecules behave, electrostatically, like spherical conductors. This allows us to develop a very simple formula for $\Delta E_n^{(Gap)}$, based upon a spherical quantum rigid rotor model for the valence electrons in the anion. The formula gives $\Delta E_n^{(Gap)}$ as a function of A_n.

Then, employing that formula for $\Delta E_n^{(Gap)}$ in Eq. (2), we are able to obtain below a simple analytic formula for I_n, which also is expressed as a function of A_n. That simple formula for I_n yields values (the open diamonds in Fig. 1), which are in both qualitative and quantitative agreement with those from very computationally intensive DFT calculations (the filled diamonds in Fig. 1). In fact, as seen in the figure and in Table I, the analytic estimate of I_n for C_{60} is closer to the experimental value ($\times$ in Fig. 1) than is the estimate from DFT.

In addition, we show below that the aforementioned analytic expressions for A_n and I_n can be applied in Eq. (1) to develop physically revealing expansions for the parameters κ and C_0 that govern the previously demonstrated [5] linear scaling of the fullerenes' quantum capacitances with their average radii:

$$C_n = \kappa R_n + C_0. \qquad (3)$$

First, however, we derive in mathematical detail the simple formulas for A_n and I_n in accordance with the qualitative prescription outlined above.

II. DERIVATION OF ANALYTIC FORMULAS FOR A_n AND I_n

To derive analytic formulas for A_n and I_n, this paper adapts to fullerene molecules prior classical electrostatic analyses [13,14] of the energetics of electron detachment in small metal particles. Because of its mobile valence π-electrons, we begin by treating a fullerene as though it were simply a
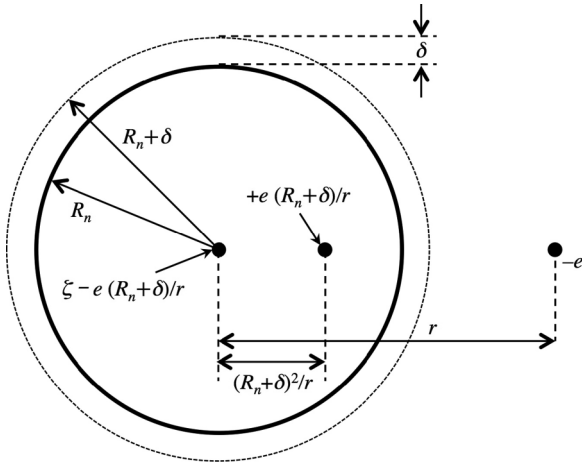
FIG. 2. Diagram of image charge model for the ionization of a fullerene anion or neutral state. See Refs. [12,13] and [14].

net neutral conducting sphere, in accordance with the diagram in Fig. 2. We take all positive charges to be on the surface of the sphere at radius R_n, while the equal number of negative charges are distributed in a thin region above and below that surface, with their positions having an average radius R_n, as well. Further, in a detachment process, an electron outside the sphere is considered to move from a radius $r = R_n + \delta$ above the spherical surface to $r = \infty$, where $0 < \delta \ll R_n$.

A. Electron affinity formula

Then, to calculate A_n, we model such a process that detaches an extra electron from the radius $r = R_n + \delta$, just outside the conducting surface within a fullerene anion. This leaves behind the neutral molecule, which we represent by constraining the surface of the sphere to always have a net charge of zero. A particular virtue of this conceptual approach is that it enables us to apply an elementary classical image charge model for a conducting sphere [12] to yield directly the formulas

$$A_n = \frac{R_n^3}{2(R_n + \delta)^2 \left[(R_n + \delta)^2 - R_n^2 \right]} \tag{4a}$$

$$\approx \frac{1}{4\delta} - \frac{5}{8}\left(\frac{1}{R_n} \right) + \frac{9}{16}\delta\left(\frac{1}{R_n} \right)^2. \tag{4b}$$

Above, Eq. (4b) is a simplification of the result of a power series expansion of Eq. (4a) taken through second order in δ/R_n.

While these equations are classical in their overall form, the distance δ is quantum mechanical in its origin, as we have noted above. Thus, the addition of this finite distance to R_n in the expression above provides a kind of quantum adaptation or correction to the simple, otherwise classical electrostatic model.

Some investigators [11,22] have expressed reservations about the application of electrostatic equations like Eqs. (4) for estimating electron affinities and ionization potentials. However, these concerns are connected to the limitations of the conducting sphere model described above when it is applied

to a solid particle, wherein there are energetic effects that have been attributed [22] to the accommodation or "solvation" of electrons in the filled interior. Such reservations do not apply to the fullerenes, quasispheres which have hollow interiors.

Thus, the simple electrostatics-like Eq. (4a) is seen in Fig. 1 and in Table I to provide an uncannily accurate approximation to values for A_n obtained from prior [5] detailed DFT calculations. In the figure, the solid circles and the lowermost solid black curve fitted to them represent the DFT values, while virtually on top of them are the open circles and bold, dashed regression curve determined from Eq. (4a). In the $n = 60$ case, the value $A_{60} = 0.105$ hartree from Eq. (4a) is even very slightly closer to the experimental value of 0.098 hartree [23] than is the DFT value of 0.107 hartree.

To obtain these values and points from Eq. (4a), we have associated the first term in Eq. (4b), the second-order series expansion of A_n, with the intercept of the second-order curve fitted to the DFT values of A_n when they are plotted versus $1/R_n$, as in Fig. 1. That intercept is the work function W_∞ for bulk graphene [5,24]:

$$0.172 \text{ hartree} = W_\infty = \frac{1}{4\delta}. \tag{5}$$

This relation enables us to evaluate $\delta = 1.45$ bohr [21] and to determine from Eq. (4a) the values of A_n presented in Fig. 1 and the fourth column of Table I. The close matches in the figure and table between the electostatics-based analytic results for A_n and those from the intensive DFT calculations are especially remarkable since electron affinities are notoriously difficult to determine both computationally and experimentally.

B. Ionization potential formula

1. Electrostatics-like contributions

Similarly, in order to calculate I_n via an electrostatic approach, we consider a process that detaches an electron from the radius $R_n + \delta$ in the neutral fullerene, yielding a cation. Throughout this process we constrain the conducting sphere that represents the cation to have a net positive charge of $\zeta = +1$. Then, using the the usual treatments [13,14] for an electron outside such a charged metal sphere or particle, this model permits us to derive an initial electrostatic formula for a fullerene ionization potential:

$$\tilde{I}_n = A_n + \frac{1}{R_n + \delta} \tag{6a}$$

$$= \frac{R_n^3}{2(R_n + \delta)^2 \left[(R_n + \delta)^2 - R_n^2 \right]} + \frac{1}{R_n + \delta}. \tag{6b}$$

The right-hand side of these equations includes only the first two terms on the right-hand side of the full, accurate ionization expansion Eq. (2). Thus, as is expected from the discussion of Eq. (2) and Fig. 1 in Sec. I, using Eqs. (6) to estimate I_n for the icosahedral fullerenes gives the results along the dotted regression line in Fig. 1, which are much too small. They fall far below those on the solid regression line for the accurate DFT values of I_n.

As stated in Sec. I and as is explored further below, the most fundamental explanation of this energy difference is

TABLE I. Closed-shell icosahedral fullerene electron detachment energies, A_n and I_n, from simple electrostatics-based theory and resulting analytic equations compared with those from DFT.

Number of carbon atoms, n	Average radius,[a] R_n (bohr)	$1/R_n$ (bohr^{-1})	Electron affinities		Ionization potentials			
			From DFT,[b] A_n (hartree)	From Eq. (4a), A_n (hartree)	From DFT,[b] I_n (hartree)	From Eq. (6b), $\tilde{I}_n$ (hartree)	From Eq. (7c),[c] I_n (hartree)	From Eq. (16), I_n (hartree)
60	6.705	0.1491	0.107	0.105	0.283	0.228	0.293	0.277
180	11.593	0.0863	0.127	0.128	0.254	0.205	0.252	0.247
240	13.366	0.0748	0.130	0.133	0.241	0.201	0.244	0.238
540	19.942	0.0501	0.144	0.145	0.222	0.192	0.223	0.218
720	22.990	0.0435	0.148	0.148	0.218	0.189	0.217	0.212
960	26.520	0.0377	0.151	0.151	0.212	0.187	0.212	0.207
1500	33.112	0.0302	0.155	0.155	0.205	0.184	0.205	0.200
2160	39.711	0.0252	0.158	0.158	0.200	0.182	0.200	0.196

[a]Average radius R_n is the arithmetic mean of distances of all carbon atoms in a fullerene from a central point within the molecule, as determined from icosahedral fullerene geometries optimized by Lewis *et al.* [5].
[b]DFT values of A_n and I_n from Ref. [5]. In the $n = 60$ case, experimental values are $A_{60} = 0.098$ and $I_{60} = 0.279$ hartree from Ref. [23].
[c]Within Eq. (7c), employed values $\kappa = 0.561$ and $C_0 = 1.58$ determined in Ref. [5].

found in the quantum mechanics that dictates the unusually large gap between the HOMO and LUMO energy levels of an icosahedral fullerene. Still, it is possible to account for and correct the disagreement between the results from Eq. (6b) and the DFT values of I_n within the framework of our electrostatics-like algebraic approach. To do so, we take advantage of the fact that the electrostatics-based Eq. (4a) is seen to be so accurate in evaluating the values of A_n. Thus we use Eq. (4a) along with Eq. (1) to write

$$I_n = A_n + \frac{1}{C_n} \tag{7a}$$

$$= \frac{R_n^3}{2(R_n + \delta)^2 \left[(R_n + \delta)^2 - R_n^2 \right]} + \frac{1}{C_n} \tag{7b}$$

$$= \frac{R_n^3}{2(R_n + \delta)^2 \left[(R_n + \delta)^2 - R_n^2 \right]} + \frac{1}{\kappa R_n + C_0}. \tag{7c}$$

The last of the set of equations above follows from Eq. (3), the highly accurate relationship for the fullerenes observed from DFT calculations in our earlier work [5]. In Eqs. (3) and (7c), the parameter κ is the analog of a dielectric constant in classical electrostatics, but for a single molecule. Though it appears to be classical, it actually is quantum mechanical in nature, as is shown below. Parameter C_0, the capacitance intercept, has no analog in classical electrostatics. Below we also express it in terms of more fundamental quantum parameters.

One may evaluate Eq. (7c) using the DFT-based values of $\kappa = 0.561$ and $C_0 = 1.58$ hartree^{-1} for the icosahedral fullerenes [5], along with the above-stated value for δ. The values thus obtained for I_n are given in column 8 of Table I. There, a very close match is seen between these capacitance-corrected electrostatic values for I_n and the DFT values in column 6 of the table. This calculation illustrates the accuracy of Eq. (7c), which can be attributed to the accuracies of Eq. (3) and Eq. (4a).

Since Eq. (7c) is so accurate in its estimate of I_n, from Eq. (2) it also must account accurately for the quantum energy gap. Within the electrostatics-like framework, one can compare Eqs. (2) and (7c) to obtain an expression for the energy gap:

$$\Delta E_n^{(\text{Gap})} = \frac{1}{\kappa R_n + C_0} - \frac{1}{R_n + \delta}. \tag{8}$$

The fact that the quantum energy gap is associated with the difference between the final terms of Eqs. (7c) and (6b) suggests that the electrostatics-like Eq. (7c) generalizes Eq. (6b) to embody quantum effects. These include especially effects arising because it has a nonzero energy gap. Such effects are embodied in the fact that $\kappa < 1$ and $C_0 \neq 0$.

Of course, in the case that $\kappa = 1$ and $C_0 = \delta$, Eq. (7c) reduces to Eq. (6b), the electrostatics-like ionization potential equation. Note, however, even in this case the result is intrinsically quantum mechanical because the capacitance intercept C_0 is nonzero.

As implied in the previous paragraph, when one considers the case where $\kappa = 1$, a comparison of Eqs. (6b) and (7c) suggests that

$$C_0 \approx \delta. \tag{9}$$

In fact, we see that in atomic units the value $C_0 = 1.58$ determined from capacitance scaling [5] is fairly close to the value $\delta = 1.45$ derived from Eq. (5) and the work function of graphene. This further affirms the accuracy of the development above.

2. Quantum contribution and ionization potential formula

While Eq. (8) provides an explanation of the quantum energy gap from within an electrostatics-like model, it does not provide a simple, independent means for calculating $\Delta E_n^{(\text{Gap})}$. We do so here by developing a very simple quantum model that takes further advantage of the fact that a neutral fullerene and its anion appear to behave much like metal quasispheres,

as we found above in the electrostatic calculation of A_n and as earlier investigators [25] also have observed. This observation suggests that we may treat the outermost, unpaired electron in the LUMO on the anion as though it were a free particle on a sphere that obeys the kinetic energy equation for a quantum rigid rotor:

$$A_n = -\varepsilon_{\text{LUMO},n} = t_{\text{LUMO},n}$$
$$= \frac{j_{\text{LUMO},n}(j_{\text{LUMO},n} + 1)}{2R_n^2}. \tag{10}$$

Above, from the virial theorem, the negative of the total one-electron energy for the LUMO in an n-carbon fullerene, $-\varepsilon_{\text{LUMO},n}$, is equal to its kinetic energy $t_{\text{LUMO},n}$, while this quantity also corresponds to the electron detachment energy A_n, as it would for any effective one-electron system [26]. In this last equation, $j_{\text{LUMO},n}$ is an integer angular momentum or "rotational" quantum number.

Similarly, the fact that a neutral fullerene appears to behave like a spherical metal shell in an image-charge model suggests that in the next one-electron energy level below the LUMO in kinetic energy, the HOMO for the neutral species, the electron is mobile and obeys a free-electron equation analogous to Eq. (10). Then, one may calculate the HOMO-LUMO energy gap simply as

$$\Delta E_n^{\text{(Gap)}} = \frac{j_{\text{LUMO},n}(j_{\text{LUMO},n} + 1)}{2R_n^2}$$
$$- \frac{j_{\text{HOMO},n}(j_{\text{HOMO},n} + 1)}{2R_n^2}. \tag{11}$$

At first, this might seem like an oversimplification, since it has been shown [15,16] that a spherical free-electron model does not accurately represent all valence π-type energy levels of an icosahedral fullerene. Further, the energy gap we propose to calculate with a spherical free-electron model in Eq. (11) is produced [16,18,20] by the very same icosahedral symmetry breaking that simultaneously renders a spherical free-electron model invalid for representing the energies of all π-type electrons in an icosahedral fullerene.

Our use of a spherical free-electron model is not actually a contradiction or oversimplification, though, because we do not assert here that *all* the fullerene's π-electron energy levels can be represented via a spherical free-electron model, as is usually done. Rather, we only assert or assume that the energy of the LUMO and the energy of separation between *two* of the highest levels, the HOMO and LUMO, may be calculated from such a model. This is consistent with earlier work [25] and observations in our electrostatic analysis above, indicating that a neutral fullerene and its anion behave like metal quasispheres, wherein at least one electron should be free to move on the surface. Thus, we only apply the spherical free-electron model in a high-energy subspace of all the fullerene's π-electron states.

In this connection, it is important to emphasize, as well, that the quantum number j we introduce in Eqs. (10) and (11) is not the same as the angular momentum quantum number (usually written l) that appears in standard free electron treatments [15–17] of the fullerenes and that counts all π-electron states. Here j counts only a few of the highest-energy valence π-electron states, as is demonstrated below.

Having explained the limitations we place upon the valence spherical free-electron model employed here, we now proceed to account for the usual condition on the HOMO and LUMO quantum numbers,

$$j_{\text{LUMO},n} = j_{\text{HOMO},n} + 1 \equiv j_n + 1, \tag{12}$$

where we also have simplified the notation by defining $j_n \equiv j_{\text{HOMO},n}$. Using Eq. (12), Eq. (11) may be simplified to read

$$\Delta E_n^{\text{(Gap)}} = \frac{j_n + 1}{R_n^2}. \tag{13}$$

Also, Eqs. (10) and (12) may be used to show that

$$\frac{1}{2R_n^2} = \frac{A_n}{(j_n + 1)(j_n + 2)}. \tag{14}$$

With the substitution of this last result in Eq. (13), after slight rearrangement one obtains the final expression for the energy gap, written as a very simple function of the quantum numbers and the electron affinity:

$$\Delta E_n^{\text{(Gap)}} = \left(\frac{2}{j_n + 2}\right) A_n. \tag{15}$$

Further, when inserted in Eq. (2), the preceding simple expression implies that a fullerene ionization potential, including its purely quantum contribution, can be written as a very simple function of the molecule's electrostatics-based electron affinity:

$$I_n = \left[1 + \left(\frac{2}{j_n + 2}\right)\right] A_n + \frac{1}{R_n + \delta}. \tag{16}$$

3. Values for the quantum numbers

To evaluate and test the simple expressions in Eqs. (15) and (16), though, one must know the values for the quantum numbers j_n (i.e., the HOMO quantum numbers). Fortunately these can be determined analytically, as follows. Since we can accurately calculate the value of A_n from the electrostatics-like equation (4a), we take A_n to be a known quantity. Then, one can rewrite Eq. (14) in the form of a quadratic equation in j_n:

$$0 = (j_n + 1)(j_n + 2) - 2R_n^2 A_n \tag{17a}$$
$$= (j_n)^2 + 3j_n + (2 - 2R_n^2 A_n). \tag{17b}$$

This equation has the *real number* solution

$$j_n^{(Real)} = -\frac{3}{2} + \frac{1}{2}[9 + 8(R_n^2 A_n - 1)]^{1/2}, \tag{18}$$

where the solution with the negative sign in front of the square root has been ruled out on physical grounds, because j_n must be a positive number. Employing this last equation and values from columns 2 and 5 of Table I, real values for $j_n^{(Real)}$ are obtained and shown in Table II, along with the values of the integers closest to them. It is these integers we take to be the actual values of the valence quantum numbers j_n for the icosahedral fullerenes.

Substituting those integral quantum number values in Eq. (15), along with the values of A_n determined from Eq. (4a), we are able to predict values for the energy gap, $\Delta E_n^{\text{(Gap)}}$ that are given in Table II. It is these predicted values of $\Delta E_n^{\text{(Gap)}}$

TABLE II. Values calculated for the HOMO-LUMO energy gap $\Delta E_n^{(Gap)}$, the valence angular momentum quantum number j_n upon which it depends, and the molecular dielectric constant κ_n for each n-carbon icosahedral fullerene.

No. carbon atoms, n	From Eq. (18), $j_n^{(Real)}$	Closest integer to $j_n^{(Real)}$, j_n	$2/(j_n + 2)$	From Eq. (15), $\Delta E_n^{(Gap)}$ (hartree)	From Eq. (22), κ_n
60	1.619	2	0.500	0.049	0.44
180	4.398	4	0.333	0.042	0.49
240	5.422	5	0.286	0.037	0.51
540	9.246	9	0.182	0.026	0.56
720	11.027	11	0.154	0.023	0.58
960	13.091	13	0.133	0.020	0.58
1500	16.952	17	0.105	0.016	0.60
2160	20.822	21	0.087	0.014	0.60

that are used in Eq. (2) to calculate the values of I_n that are presented in Table I and plotted as the open diamonds versus $1/R_n$ in Fig. 1. From the close match of these predicted values for I_n with the DFT results (filled diamonds), it is seen how accurate are the formulas derived here in Eqs. (15), (16), and (18).

4. Example of energy gap and ionization potential formulas for $n = 60$

To highlight the great simplification implicit in Eqs. (15) and (16), it is useful to consider a specific example. Take the case of the well-studied "buckyball," for which $n = 60$. In that case, as seen in Table II, $j_{60} = 2$. Substitution of this value for the quantum number in Eqs. (15) and (16) gives, respectively, the HOMO-LUMO energy gap and ionization potential for C_{60} simply as

$$\Delta E_{60}^{(Gap)} = \tfrac{1}{2} A_{60} \qquad (19)$$

and

$$I_{60} = \frac{3}{2} A_{60} + \frac{1}{R_{60} + \delta}. \qquad (20)$$

This last equation is very accurate, producing a value $I_{60} = 0.277$ hartree that is closer to the experimental value [23], 0.279 hartree, than is the DFT value [5] of 0.283 hartree. This further illustrates the accuracy of the analytic results in Secs. II B 2 and II B 3, as well as the likely accuracy of the free-electron assumptions that were made to derive them.

III. ANALYSIS OF THE MOLECULAR CAPACITANCES

In a series of prior investigations [5–9], it has been demonstrated empirically that the quantum capacitances of atoms and molecules scale linearly with their effective radii, in accordance with two-parameter relations much like Eq. (3). However, in that earlier work no first-principles equations were presented to explain or predict the nature and the values of the two fundamental scaling parameters κ and C_0.

Above, in Eq. (9), we now have provided such a first-principles explanation for the capacitance intercept C_0, at least in the case of the icosahedral fullerenes. In this section, we build upon that to explain, as well, the nature of the molecular

dielectric constant κ. We also show here that the molecular capacitance C_n consists of two contributions, one of which is essentially electrostatic and quasiclassical, while the other is strictly quantum mechanical in origin.

A. Evaluation of the molecular dielectric constant κ in terms of the quantum numbers

From the development in Sec. II, we have an accurate expression, Eq. (8), for the fullerene's HOMO-LUMO energy gap from an electrostatic point of view and another, Eq. (15), from a quantum mechanical point of view. The former involves the molecular dielectric constant κ, while the latter is given in terms of the quantum number j_n. These two expressions may be used to expand κ in terms of j_n. To do so, first let us eliminate $\Delta E_n^{(Gap)}$ between them:

$$\frac{1}{\kappa R_n + \delta} \approx \left(\frac{2}{j_n}\right) A_n + \frac{1}{R_n + \delta}, \qquad (21)$$

where we have used Eq. (9) to substitute δ for C_0, which makes the relation above only approximate. This last equation may be rearranged to yield

$$\kappa_n \approx \frac{1}{R_n}\left[\frac{j_n(R_n + \delta)}{2A_n(R_n + \delta) + j_n}\right] - \frac{\delta}{R_n}. \qquad (22)$$

The dependence of this equation upon the quantum number j_n suggests an explanation for the discretization or "quantization" seen [6] in the values of κ for other spherical quantum systems, notably atoms.

Of course, the dielectric constant should be just that, a constant, for all n, as it was determined to be in our prior work [5]. However, because of the n dependence of the right-hand side of Eq. (22) it has been necessary to add a subscript n to κ on the left-hand side of the equation, suggesting it has a similar dependence on n. This judgment is borne out by the variation seen in κ_n when the equation is evaluated, as it is in the rightmost column of Table II.

Consistent with our prior analysis [5] of κ via polynomial expansions of the detachment energies about $(1/R_n) = 0$, one way to eliminate the n dependence in the expansion here of the dielectric constant is to consider it in the limit as R_n becomes very large. In that limit Eq. (18) becomes

$$j_n^{(Real)} \approx R_n(2A_n)^{1/2}, \qquad (23)$$

so that the limiting form of Eq. (21) becomes

$$\frac{1}{\kappa R_n} \approx \frac{(2A_n)^{1/2}}{R_n} + \frac{1}{R_n}. \qquad (24)$$

In addition, from Eq. (4b) with R_n very large, we have $A_n = 1/4\delta$, as is also implicit in Eq. (5).

When one substitutes this limiting expression for A_n in the limiting relation Eq. (24) and solves for κ, then applies the value $\delta = 1.45$ bohr from Eq. (5), the results are

$$\kappa \approx \frac{1}{1 + (1/2\delta)^{1/2}} = 0.63, \qquad (25)$$

in the limit of very large R_n. This limiting value of κ is consistent with the progression of values for κ_n seen in Table II. Also, the limiting value agrees to one decimal place (i.e., $\kappa \approx 0.6$) with the value $\kappa = 0.56$ determined from prior regression

analysis [5] of DFT-determined quantum capacitances, which is encouraging.

Even so, it would be more appropriate to compare the value of κ from our theoretical analysis above to the value arising from a different linear regression upon capacitances versus fullerene radii. That would be one in which the capacitances are not calculated from DFT detachment energies, but from the accurate detachment energies that are determined from the theoretical equations (4a) and (16) derived here. To do so, we use in Eq. (1) the values of A_n and I_n from columns 5 and 9, respectively, of Table I. When the resulting theoretical values of C_n are plotted versus the corresponding values of R_n from column 2 of the table, the regression equation is $C_n = 0.628 R_n + 1.315$, with $R^2 = 0.9995$. That is, from the detailed regression analysis using the theoretical capacitances we obtain the result $\kappa = 0.628$. This agrees precisely with the limiting result of Eq. (25) and constitutes an even more persuasive demonstration of the accuracy of the limiting analysis above.

In considering the estimates of κ from the regressions, though, it is noteworthy that the capacitance expansions $1/(I_n - A_n)$ can have small denominators. Hence, they will be sensitive to even very small differences or errors in the theoretical estimates of I_n and A_n, as will the resulting slope of their regression line versus R_n. For this reason, we take as a considerable success the agreement of our theoretical estimate of slope κ with the DFT estimate to one decimal place, $\kappa = 0.6$.

B. Two capacitances connected in series

The authors have observed that many investigators present formulas and calculations of capacitances for atomic and molecular scale quantum systems or clusters of such systems. Often, though, other works do not clarify or show an awareness of which portion of the capacitance is being estimated. Thus, here, we wish to use the results given above to show explicitly that the total capacitance of such a quantum system actually consists of two capacitances that are effectively connected in series.

First, we observe that the total capacitance calculated above in terms of Eq. (3) and which appears in the denominator in Eq. (7c) differs from the capacitance

$$C_n^{(ES)} = R_n + \delta \qquad (26)$$

that prior investigators [11,19] have identified as being associated with the electrostatic (ES) energy for charging a small metal particle. In terms of $C_n^{(ES)}$, the usual, more nearly classical estimate of the ionization potential $\tilde{I}_n$, in Eq. (6), may be restated:

$$\tilde{I}_n = A_n + \frac{1}{C_n^{(ES)}}, \qquad (27)$$

in analogy with Eq. (7a). Additionally, taking account of the difference ΔI_n between an accurate value of I_n and $\tilde{I}_n$, we define the capacitance associated with this energy difference due to quantum (Q) effects:

$$C_n^{(Q)} = \frac{1}{\Delta I_n} \equiv \frac{1}{I_n - \tilde{I}_n}. \qquad (28)$$

Using Eqs. (27) and (28) within the definition Eq. (1), we can show that the total quantum capacitance C_n may viewed as consisting of two capacitances, $C_n^{(ES)}$ and $C_n^{(Q)}$, that combine according to the series capacitance combination relation [27]:

$$C_n = \frac{1}{(\tilde{I}_n - A_n) + (I_n - \tilde{I}_n)} \qquad (29a)$$

$$= \frac{1}{1/C_n^{(ES)} + 1/C_n^{(Q)}}. \qquad (29b)$$

Thus, as asserted above, the *total* quantum capacitance C_n effectively consists of two component capacitances, an electrostatic contribution to the total capacitance and a quantum contribution that are effectively connected in series.

Further, it is shown in preceding sections of this work that the quantum contribution for the fullerenes is directly related to the HOMO-LUMO quantum energy gap $\Delta E_n^{(Gap)}$, since for these molecules $(I_n - \tilde{I}_n) = \Delta E_n^{(Gap)}$ and

$$C_n^{(Q)} = \frac{1}{\Delta E_n^{(Gap)}} \qquad (30)$$

from Eqs. (28), (2), and (6a). This finding is consistent with that of Luo *et al.* [19].

For a true metal particle, $\Delta E_n^{(Gap)}$ is very small (i.e., effectively zero) so $I_n - \tilde{I}_n$ is usually very small, as well. Thus, this quantum contribution to total capacitance C_n can be negligible. However, for an atom or molecule, even a conductive one, the HOMO-LUMO gap usually is significant, as it is for the fullerenes. In such cases, purely classical estimates of the capacitance are not accurate.

IV. DISCUSSION: OPEN-SHELL ICOSAHEDRAL FULLERENES

As noted in the Introduction, the icosahedral fullerenes to which our electrostatics-based theory has been applied above have the chemical formula C_{60k}. These possess closed-shell neutral states [2]. However, the essential ideas of the analysis also can be applied to other icosahedral fullerenes having the chemical formula C_{60k+20}. We accomplish this by recognizing that these other icosahedral fullerene structures have open-shell neutral states [2].

Unlike the situation described in Secs. I and II for closed-shell species, an additional electron still can be placed in the energy level of the HOMO when that electron is added to an open-shell neutral fullerene to form its anion. Thus, a large energy gap of the sort displayed in Fig. 1 will not be present to add to the energy separating I_n and A_n in the open-shell species; that is, $\Delta E_n^{(Gap)} \approx 0$. Thus, from Eq. (2), we expect that

$$I_n - A_n \approx 1/(R_n + \delta). \qquad (31)$$

Then, from the definition, Eq. (1), the capacitance of the open-shell species should be approximated by $C_n^{(ES)}$, in accordance with Eq. (26).

Though few results on the detachment energies and dimensions of these open-shell fullerenes are available in the literature, the preceding proposition can be tested numerically in the case of the open-shell icosahedral fullerene C_{320}. From

Lewis *et al.* [5], we have the DFT results $A_{320} = 0.1543$ hartree, $I_{320} = 0.2107$ hartree, and $C_{320} = 17.72$ hartree^{-1} for a C_{320} structure with an average radius $R_{320} = 15.19$ bohr. By comparison, substitution of this value for R_{320} in Eq. (26) gives the capacitance 16.64 hartree^{-1}. This electrostatics-based calculation underestimates the DFT result for C_{320} by only 6.1%, lending credence to the approximate analysis immediately above.

Further confirmation comes from using the value above for R_{320} in Eq. (4a) and then employing Eq. (2) with $\Delta E_n^{(\text{Gap})} = 0$, which produce the electrostatics-based approximations $A_{320} = 0.1371$ hartree and $I_{320} = 0.1972$ hartree, respectively. These underestimate the corresponding DFT values by only 11.1 and 6.4%. Overall, the electrostatics-based results for the open-shell C_{320} system do not correspond as closely to the DFT values as do those in Table I and Fig. 1 for the closed-shell icosahedral fullerenes, but they do suggest that the essential elements of the analysis here apply, at least approximately, to both types of icosahedral fullerenes.

V. SUMMARY AND CONCLUSIONS

To summarize, in this paper we have derived two simple analytic formulas, Eqs. (4a) and (16), that evaluate with great accuracy the electron affinities A_n and ionization potentials I_n for n-carbon, closed-shell icosahedral fullerenes, as is illustrated in Fig. 1. This is notable because the accurate determination of such electron detachment energies usually requires long, computationally intensive quantum mechanical calculations using complex computer codes and because the formula for A_n is derived using a fundamentally classical electrostatic approach.

Even more notable is that, although the larger ionization potentials are more frequently and easily calculated in conventional quantum theoretical and quantum computational approaches, here we find the smaller, electrostatically derived electron affinities to be in a certain way more fundamental. This is because, through Eqs. (2) and (15), the fullerenes' ionization potentials may be expressed in Eq. (16) as a simple function of their electron affinities, their dimensions, and a rotational quantum number j_n for the highest occupied molecular orbital. Further, the value of this quantum number may be determined analytically via Eq. (18) for each fullerene and is also seen to be a function of the electron affinity and the dimensions of the molecule.

It is pointed out, though, that despite the classical derivation of the electron affinity formula (4a), it also is quantum mechanical in nature because of the incorporation in it of a quantum length parameter δ. The value of δ is constant for all the icosahedral fullerenes and determined via Eqs. (4b) and (5) from the work function of graphene (i.e., essentially a fullerene with $n = \infty$). Thus, the quantum effects that are embodied in

δ, along with the fullerenes' dimensions, dictate the values of A_n and are shown here also to dictate those for I_n.

Another unique aspect of the calculation of the electron detachment energies here is the isolation of all the many-electron contributions to I_n and A_n in quasiclassical terms arising in the electrostatic image charge formula (4a). This takes advantage of effects embodied in the quantum length parameter δ so that the energies are parsed with the only explicitly quantum mechanical terms, those within $\Delta E_n^{(\text{Gap})}$, accounting just for one-electron kinetic energies.

Here, as well, the analytic formulas for I_n and A_n are applied to resolve a long-standing question concerning the molecular quantum capacitance. Specifically, from these formulas and the definition of the quantum capacitance in Eq. (1), analytic equations are derived to determine from first principles the fundamental slope and intercept parameters, κ and C_0, that govern linear scaling of the quantum capacitance through Eq. (3). In a series of papers [5–9], these scaling parameters had been evaluated empirically and shown to have discrete or "quantized" values, but the underlying physics and rationale for these properties had not been revealed until now.

Despite this overall quantization, it also is shown above that the parsing of I_n into a sum of two primarily classical electrostatic contributions and a primarily quantum contribution, as described in Eq. (2), similarly parses the total capacitance of a fullerene into a classical component and a quantum component. These two component capacitances are shown in Eq. (29b) to be effectively connected in series to produce the total capacitance of a fullerene as calculated via Eq. (1).

Even more generally interesting is the way in which I_n and A_n are shown to be coupled in Eq. (16). This is a step toward a more general understanding of the way in which the energy of an $(N+1)$-electron system or that of an $(N-1)$-electron system are determined directly by the structure of the corresponding N-electron system.

In future investigations, the authors hope to explore the extent to which the insights gained here and enumerated above can be applied to nanoscale and quantum systems other than fullerenes. In addition, as pointed out in the Introduction, since there are increasing efforts to make industrial use of nanoscale carbon particles, it will be of interest to see how the present work can inform their applications.

[1] M. S. Dresselhaus, G. Dresselhaus, and P. C. Eklund, *Science of Fullerenes and Carbon Nanotubes* (Academic Press, New York, 1996).

[2] P. W. Fowler and D. E. Manolopoulos, *An Atlas of Fullerenes* (Dover, New York, 2006). See esp. p. 51 for a discussion of closed versus open-shell icosahedral fullerene structures.

[3] H. D. Abruña, Y. Kiya, and J. C. Henderson, Phys. Today **61**(12), 43 (2008).

[4] M. S. Halper and J. C. Ellenbogen, *Supercapacitors: A brief overview*, Technical Report MP 05W0000272 (MITRE Corp., McLean, Virginia), https://www.mitre.org/sites/default/files/pdf/06_0667.pdf.

[5] G. R. Lewis, W. E. Bunting, R. R. Zope, B. I. Dunlap, and J. C. Ellenbogen, Phys. Rev. A **87**, 052515 (2013).

[6] J. C. Ellenbogen, Phys. Rev. A **74**, 034501 (2006).

[7] J. C. Ellenbogen, C. A. Picconatto, and J. S. Burnim, Phys. Rev. A **75**, 042102 (2007).

[8] J. C. Ellenbogen, Phys. Rev. A **82**, 012508 (2010).

[9] W. E. Bunting and J. C. Ellenbogen, Phys. Rev. A **85**, 062503 (2012).

[10] G. J. Iafrate, K. Hess, J. B. Krieger, and M. Macucci, Phys. Rev. B **52**, 10737 (1995).

[11] J. P. Perdew, Phys. Rev. B **37**, 6175 (1988).

[12] L. D. Landau, E. M. Lifschitz, and L. P. Pitaevskii, *Electrodynamics of Continuous Media*, 2nd ed. (Elsevier Butterworth-Heinemann, Oxford, 1984). See esp. pp. 9–10.

[13] D. M. Wood, Phys. Rev. Lett. **46**, 749 (1981).

[14] M. P. J. van Staveren, H. B. Brom, L. J. de Jongh, and Y. Ishii, Phys. Rev. B **35**, 7749 (1987).

[15] M. Ozaki and A. Takahashi, Chem. Phys. Lett. **127**, 242 (1986).

[16] K. Yabana and G. F. Bertsch, Phys. Scr. **48**, 633 (1993).

[17] C. Yannouleas and U. Landman, Chem. Phys. Lett. **217**, 175 (1994).

[18] F. Rioux, J. Chem. Educ. **71**, 464 (1994).

[19] J. Luo, Z. Q. Xue, W. M. Liu, J. L. Wu, and Z. Q. Yang, J. Phys. Chem. A **110**, 12005 (2006).

[20] P. W. Fowler and T. Pisanski, Acta Chim. Slov. **57**, 513 (2010).

[21] It may be seen that the value $\delta = 1/4W_\infty = 1.45$ bohr is a physically reasonable estimate of the added radius for the attachment or detachment of a valence electron to or from a fullerene, as asserted in Sec. I, by recognizing that δ closely approximates the average, 1.5 bohr, of a carbon atom's Hartree-Fock valence mean radius $\langle r \rangle = 1.71$ bohr with its Bohr radius $\langle 1/r \rangle^{-1} = 1.28$ bohr.

[22] G. Makov, A. Nitzan, and L. E. Brus, J. Chem. Phys. **88**, 5076 (1988), and references cited therein.

[23] P. J. Linstrom and W. G. Mallard (eds.), *NIST Chemistry WebBook*, NIST Standard Reference Database No. 69 (National Institute of Standards and Technology, Washington, DC, 2016), http://webbook.nist.gov/chemistry.

[24] S. Suzuki, C. Bower, Y. Watanabe, and O. Zhou, Appl. Phys. Lett. **76**, 4007 (2000).

[25] H. Zettergren, B. O. Forsberg, and H. Cederquist, Phys. Chem. Chem. Phys. **14**, 16360 (2012).

[26] M. Karplus and R. N. Porter, *Atoms and Molecules* (Addison-Wesley, New York, 1970).

[27] D. Halliday, R. Resnick, and J. Walker, *Fundamentals of Physics*, 6th ed. (Wiley, New York, 2001).